Diffraction by Sharp Edges of Noncanonical Shape with Mean Flow and Surface Impedance

Yueping Guo[1]
NASA Langley Research Center

This paper presents a study on diffraction by sharp edges of noncanonical edge shape in the presence of mean flow and surface impedance, which are important features for aircraft noise but have not been accounted for in previous studies on sharp-edge diffraction. An analytical formula for the diffracted pressure is derived by applying asymptotic analysis to the integral representation of the total pressure scattered by a geometry that contains sharp edges. The asymptotic analysis is presented as a systematic process that can be carried out to any order, if needed. An illustration is given to use a higher-order result to eliminate the singularity in the first-order result to make the solution regular in the entire parameter domain. The formula for the diffracted pressure is validated by experimental data and is applied to parametric studies to reveal the effects of noncanonical edge shape, mean flow and surface impedance, as well as the impact of these effects on the total scattered pressure in the presence of other scattering components.

Nomenclature

A = amplitude quantity in diffracted pressure
C_D = diffraction coefficient
C_R = reflection coefficient
c_0 = mean sound speed
f = integrand function
F = Fresnel function
G = Green's function
k_0 = acoustic wavenumber
$\mathbf{M}$ = Mach number vector
$\mathbf{n}$ = unit surface normal vector
$\mathbf{n}_c$ = unit principal normal of edge shape
p = acoustic pressure
p_D = diffracted acoustic pressure
p_I = incident acoustic pressure
q_0 = source strength
R = surface element to microphone distance modified by flow
R_s = surface element to source distance modified by flow
s = arc length coordinate
s^* = arc length coordinate at diffraction point
$\mathbf{s}$ = arc length coordinate unit vector
S = scattering body surface
s_i = surface curvilinear coordinates (i=1,2)
$\mathbf{w}$ = auxiliary vector related to microphone
$\mathbf{w}_s$ = auxiliary vector related to source
$\mathbf{x}$ = field coordinates
$\mathbf{x}_s$ = source location coordinates
$\mathbf{y}$ = surface coordinates
$\mathbf{y}^*$ = stationary point coordinates
Z = surface impedance

---

[1] Senior Research Engineer, Aeroacoustics Branch, AIAA Associate Fellow, Seal Beach, CA 90740, USA.

β = Mach number factor
δ = Dirac delta function
Δ = denominator in diffracted pressure
η = transformation variable
κ_0 = modified acoustic wavenumber
ρ_0 = mean density
ω = angular frequency
Φ = acoustic wave phase function at microphone
Φ_s = acoustic wave phase function from source
Ψ = phase function of integrand function
Ψ_0 = phase function of integrand function at singularity

I. Introduction

Sound diffraction by sharp edges has been studied for canonical geometries such as semi-infinite plates and infinite wedges, where the diffraction occurs on an infinite long straight line [1-10]. These studies have been exclusively for rigid surfaces in static media, probably because of their original applications in radar scattering. The results from such problems have been used to approximate geometries that may only slightly deviate from the canonical geometries [11-18], plates of large dimensions with long straight edges, for example. This has been valuable in aircraft noise applications in some configurations such as the trailing edges of an aircraft wing where some segments of the edges are approximately straight over the length of many acoustic wavelengths and the chord length of the wing is also large compared with the acoustic wavelength. The approximations are clearly very restrictive, requiring the edges to be straight in shape, the diffraction to be in static media without mean flow, and the scattering geometry to be rigid without surface treatment. There are many applications in aircraft noise scattering where all or some of these requirements are not satisfied, chevron nozzles on the exhaust of aircraft engines being one example and the lower edges of engine pylons being another. Some unconventional aircraft such as the blended-wing-body aircraft also have curved trailing edge segments and potentially acoustic liner treatment on the aircraft body [19-22]. These examples illustrate three important features in aircraft noise diffraction, namely, the noncanonical edge shapes, the presence of mean flow, and the potential acoustic liner treatments on the edges for noise reduction, which are not accounted for in classical diffraction studies.

Considering the extensive studies of diffraction by canonical geometries in the past, it is natural to ask if the methods used in these studies can be extended to include the three important features for aircraft noise applications. This turns out to be very challenging, if feasible at all. The main reason for the previous studies being almost exclusively confined to canonical configurations is that each problem requires a method particularly suited to the canonical geometry and the idealized diffraction environment to derive the respective solutions, e.g., the Wiener-Hopf factorization for the semi-infinite plate [1, 5, 8] and the image source synthesis of the wedge problem [2, 3, 6]. These methods are very restrictive and cannot be extended and generalized. The method based on Kirchhoff integration [14-16] can, in principle, be used for edges of noncanonical shapes but has been shown to underpredict the diffracted sound levels [17]. Furthermore, the method is based on various heuristic approximations to force the integrand function into a form suitable for the Stokes theorem, which restricts the applications to static media and rigid surfaces.

In this paper, a general solution for sharp-edge diffraction will be presented, including the three important features. The basic formulation is the convective wave equation with impedance boundary conditions on the scattering surfaces of arbitrary shape, which may include sharp edges of any shape and orientation. The basic formulation can be converted to a surface integral representation by the standard Green's theorem. The method of asymptotic analysis [23-25] will then be used to solve the surface integral and analytically extract the diffracted sound by sharp edges from the total solution represented by the surface integral solution. The asymptotic analysis is in the high-frequency limit, with the ratio of the acoustic wavelength to the typical dimension of the scattering body as the expansion parameter. In practical applications of noise scattering for large commercial transports, the acoustic wavelength is mostly smaller than the dimensions of the aircraft components and the edge length so that the first-order solution in the asymptotic analysis is sufficient. Furthermore, the solution is not restricted to the first order. The asymptotic method is systematic and can be successively applied to derive solutions to any higher order, if needed. The solution, in explicit analytical form, is general and is a function of the edge shape, the mean flow Mach number and the surface impedance, as well as other conventional parameters such as frequency, source characteristics and microphone locations. The systematic use of the higher-order asymptotic expansion can also be used to eliminate mathematical singularities in the first-order solution to make it uniformly valid in the parametric domains.

To illustrate the effects of various features on sharp-edge diffraction, the sound scattering by an un-swept NACA 0012 airfoil will be studied, with its trailing edge designed to have various wavy shapes, as well as a straight edge as the baseline configuration, which will not only serve as a reference for comparisons but also allow for validation by experimental data available from a previous experimental study [26] to establish the accuracy of the derived solution. The airfoil geometry is simple but contains all the essential scattering mechanisms, including reflection from a curved surface, diffraction from smooth geometry at its leading edge, and sharp-edge diffraction at its trailing edge, which provide a good configuration to study various features of the sharp trailing edge and their interactions with other scattering components. The parametric studies will include replacing a portion of the straight trailing edge by wavy shapes placed at various positions in the flow direction and will include variations in the mean flow Mach number and acoustic treatment on the edge.

Comparisons will be presented between wavy edges and the baseline straight edge to show the edge-shape effect, revealing the potential for diffraction reduction by edge-shape modification and the pitfalls to avoid increase in diffraction. The impact of the sharp-edge diffraction to the total scattering depends on the presence of other scattering components and their relative ranking order of importance, including other diffraction components, as well as the direct radiation from the source and the reflection from the scattering body, which will be illustrated by the scattered sound in both the shadow where diffraction dominates and the insonified region where the direct radiation and reflection dominate. The impact also depends on the coherence characteristics of the sources. For incoherent sources, the effects of the edge features only affect the diffraction amplitudes with the diffracted acoustic energy independently added to other scattering components. For coherent sources, various components interfere with each other, leading to scattering patterns with peaks and dips. In this case, the edge features can significantly shift the scattering pattern, resulting in significant changes in the levels of the scattered sound. The comparisons of edge diffraction at various values of the flow Mach number will show the mean flow effects and illustrate this source coherence effect. The reduction of sharp-edge diffraction can be achieved by acoustic treatment on the edge, which will be demonstrated by comparisons of results with and without surface impedance.

II. Formulation

Sound diffraction by sharp edges of noncanonical shapes in the presence of mean flow and with surface impedance can be formulated by the convective wave equation in the frequency domain with impedance boundary conditions on the scattering body surface. The acoustic pressure is governed by the standard convective wave equation,

$$\nabla^2 p - \left(-\mathrm{i}k_0 + \mathbf{M}\cdot\nabla\right)^2 p = q_0\delta(\mathbf{x}-\mathbf{x}_s) \tag{1}$$

in which the acoustic pressure is denoted by p, the frequency is represented by the acoustic wavenumber, $k_0=\omega/c_0$, with ω and c_0 being the angular frequency and the mean sound speed, respectively, the mean flow is specified by the Mach number vector $\mathbf{M}$, and a point source is defined by the Dirac delta function δ, located at $\mathbf{x}_s$ with amplitude q_0. Solutions to this equation are subject to the boundary condition on the scattering body surfaces. It is convenient and useful to allow potential acoustic treatment on local areas of the surfaces, typically described as the surface impedance condition written as

$$\frac{\rho_0 c_0}{\mathrm{i}k_0 Z}\left(-\mathrm{i}k_0 + \mathbf{M}\cdot\nabla\right)^2 p + \mathbf{n}\cdot\nabla p = 0 \quad \text{on} \quad S \tag{2}$$

where ρ_0 is the mean density, Z is the surface impedance as a function of frequency, $\mathbf{n}$ is the unit normal vector of the body surface pointing into the acoustic medium, and S collectively denotes the scattering surface.

The scattering geometry is illustrated in Fig. 1 with emphasis on the three features that are important to aircraft noise, namely, the noncanonical edge shape, the presence of mean flow and the potential for acoustic treatment on the surface represented by surface impedance. The noise source, located at the point $\mathbf{x}_s$, the outward surface normal $\mathbf{n}$, and the curvilinear coordinates on the surface, s_1 and s_2, are also illustrated in the figure. The surface S is a function of the surface coordinate $\mathbf{y}$ represented by the two curvilinear coordinates, s_1 and s_2.

In general, both the Mach number and the surface impedance can depend on the spatial coordinates, the former because of nonuniform flows and the latter due to locally treated surfaces. In the framework of high-frequency asymptotic analysis to be discussed in later sections, however, variations of both are assumed to be gradual, compared to the sound wave variations within a wavelength. Furthermore, the diffraction of the incident waves is a local feature occurring at the sharp edge. The results to be derived will also show that the diffracted pressure is determined by the diffraction points on the edge, and thus, only the local quantities near the diffraction point are relevant. Thus, both these parameters can be treated as locally invariant, and the governing equations are to be solved for results in local regions. For the same reason, the Mach number vector is considered as parallel to the local surface tangential plane.

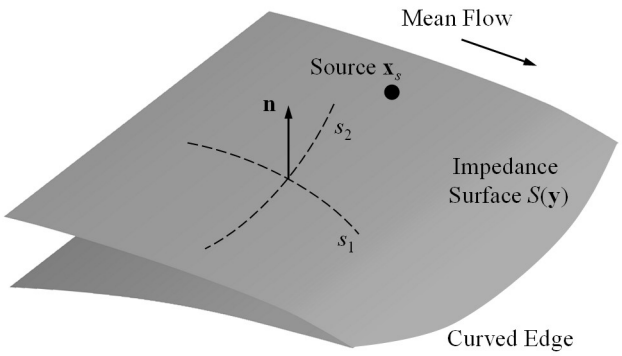

Fig. 1 Illustration of diffraction by edges of noncanonical shape with mean flow and surface impedance.

By following the standard approach of the Green's theorem, the solution that is subject to the radiation condition in the far field can be derived in terms of an integral equation,

$$p(\mathbf{x}) = p_I(\mathbf{x}) + \int_{S(\mathbf{y})} \left(p\mathbf{n}\cdot\nabla G - G\mathbf{n}\cdot\nabla p \right) ds_1 ds_2 \,, \tag{3}$$

in which S is the collection of all surfaces that can be closed or open, ∇ is the gradient operation with respect to the surface coordinates $\mathbf{y}$ on the surface, p_I is the incident field from the source, and G is the free space Green's function given by

$$G(\mathbf{x}-\mathbf{y}) = \frac{1}{4\pi R} e^{ik_0\Phi} \tag{4}$$

where R denotes the radius of curvature of the wave front, at the field point $\mathbf{x}$, of the waves generated by a source at $\mathbf{y}$ in the presence of mean flow, and Φ is the phase function of the sound waves. Both depend on $\mathbf{x} - \mathbf{y}$, given by

$$R(\mathbf{x}-\mathbf{y}) = \sqrt{\beta^2 |\mathbf{x}-\mathbf{y}|^2 + \left((\mathbf{x}-\mathbf{y})\cdot\mathbf{M}\right)^2} \quad \text{and} \quad \Phi(\mathbf{x}-\mathbf{y}) = \frac{1}{\beta^2}\left[R - \mathbf{M}\cdot(\mathbf{x}-\mathbf{y})\right] \tag{5}$$

with β^2 denoting 1-$\mathbf{M}\cdot\mathbf{M}$. The integration in the result (3) over the surface S has been written out explicitly in terms of the two orthogonal curvilinear coordinates on the surface, namely, s_1 and s_2, as shown in Fig. 1. Thus, the surface coordinate vector $\mathbf{y}$ becomes a function of these two arc length parameters, $\mathbf{y} = \mathbf{y}(s_1, s_2)$.

The gradient of the acoustic pressure in the integral equation (3) is related to the pressure by the boundary condition (2) so that by simple substitution, the result (3) becomes,

$$p(\mathbf{x}) = p_I(\mathbf{x}) + \int_{S(\mathbf{y})} \left(\mathbf{n}\cdot\nabla G + G\frac{\rho_0 c_0}{ik_0 Z}\left(-ik_0 + \mathbf{M}\cdot\nabla\right)^2 \right) p(\mathbf{y}) ds_1 ds_2 \,. \tag{6}$$

The total acoustic pressure, present on both sides of the integral equation, can be formally decomposed as the sum of an incident field from the source and scattered components due to the body, which may contain various components, including reflection, smooth-geometry diffraction and sharp-edge diffraction [17]. Thus, the total pressure on the left-hand side of (6) can be written as a sum of various components, of which, the incident field cancels the same quantity on the right-hand side. Furthermore, the surface integral on the right-hand side of this result is formally for the total scattered pressure, including the reflected component, which cancels the reflected pressure on the left-hand side. The diffracted pressure p_D can then be formally written as

$$p_D(\mathbf{x}) = \int_{S(\mathbf{y})} \left(\mathbf{n}\cdot\nabla G + G\frac{\rho_0 c_0}{ik_0 Z}\left(-ik_0 + \mathbf{M}\cdot\nabla\right)^2 \right) p(\mathbf{y}) ds_1 ds_2 \tag{7}$$

with the understanding that the surface integral should be carried out only to extract the diffraction contributions.

The acoustic pressure on the body surface in general includes contributions from the incident waves, the reflected waves, and the diffracted waves. The latter two can be expressed in terms of the incident pressure multiplied by the reflection and the diffraction coefficient, respectively. Thus, the result (7) can be rewritten as

$$p_D(\mathbf{x}) = \int_{S(\mathbf{y})} \left(\mathbf{n}\cdot\nabla G + G\frac{\rho_0 c_0}{ik_0 Z}\left(-ik_0 + \mathbf{M}\cdot\nabla\right)^2 \right) \left(1 + C_R + C_D\right) p_I(\mathbf{y}) ds_1 ds_2 \tag{8}$$

where C_R and C_D are respectively the reflection and the diffraction coefficients that are in general a function of the geometry, the mean flow, the surface impedance, and other parameters. The former is derived in [17] and the latter is an unknown but can either be found by formally carrying out the asymptotic analysis to reduce this result to an

algebraic equation to solve for the diffraction coefficient, similar to the process in [17] for the reflection coefficient, or be omitted because it is asymptotically a smaller term than the others in the result, as will be shown in the next section.

To proceed, the Greens function given by (4) can be substituted into the integrand function, together with the incident pressure which is simply the solution of the convective wave equation (1) in free space, given by

$$p_I(\mathbf{y}-\mathbf{x}_s)=\frac{q_0}{4\pi R_s}e^{\mathrm{i}k_0\Phi_s} \tag{9}$$

where R_s denotes the radius of curvature of the incident wave front, at the field point **y,** of the waves generated by a source at $\mathbf{x}_s$ in the presence of mean flow, and Φ_s is the phase function of the incident waves. They are defined similarly to R and Φ by (5), given by

$$R_s(\mathbf{y}-\mathbf{x}_s)=\sqrt{\beta^2\left|\mathbf{y}-\mathbf{x}_s\right|^2+\left((\mathbf{y}-\mathbf{x}_s)\cdot\mathbf{M}\right)^2}\quad\text{and}\quad \Phi_s(\mathbf{y}-\mathbf{x}_s)=\frac{1}{\beta^2}\left[R_s-\mathbf{M}\cdot(\mathbf{y}-\mathbf{x}_s)\right], \tag{10}$$

With these, the result (8) becomes,

$$p_D(\mathbf{x})=\frac{\mathrm{i}\kappa_0 q_0 e^{-\mathrm{i}\kappa_0(\mathbf{x}-\mathbf{x}_s)}}{(4\pi)^2}\int_{S(\mathbf{y})}\frac{1}{R_s R}\left[\mathbf{n}\cdot\mathbf{w}+\frac{\rho_0 c_0}{\beta^2 Z}\left(\frac{\nabla\cdot\mathbf{w}_s}{\mathrm{i}\kappa_0}+\left|\mathbf{w}_s\right|^2\right)\right]\left(1+C_R+C_D\right)e^{\mathrm{i}\kappa_0(R+R_s)}ds_1ds_2 \tag{11}$$

in which $\kappa_0=k_0/\beta^2$ is the acoustic wavenumber slightly modified by the mean flow, and the vectors $\mathbf{w}$ and $\mathbf{w}_s$ are,

$$\mathbf{w}=\left(1-\frac{1}{\mathrm{i}\kappa_0 R}\right)\nabla R+\mathbf{M}\quad\text{and}\quad \mathbf{w}_s=\left(1-\frac{1}{\mathrm{i}\kappa_0 R_s}\right)\nabla R_s-\mathbf{M} \tag{12}$$

which involve the gradient of R and R_s, both of which can be easily calculated from the definitions of these quantities.

The terms in the integrand function in the result (11), including those in the quantities $\mathbf{w}$ and $\mathbf{w}_s$, are conveniently expressed by the inverse of the acoustic wavenumber, equivalent to the inverse of frequency. To the leading order in the high-frequency limit, terms proportional to $1/\kappa_0$ can be neglected, leading to

$$p_D(\mathbf{x})=\frac{\mathrm{i}\kappa_0 q_0 e^{-\mathrm{i}\kappa_0(\mathbf{x}-\mathbf{x}_s)}}{(4\pi)^2}\int_{S(\mathbf{y})}\frac{1}{R_s R}\left[\mathbf{n}\cdot\nabla R+\frac{\rho_0 c_0}{\beta^2 Z}\left|\nabla R_s-\mathbf{M}\right|^2\right]\left(1+C_R+C_D\right)e^{\mathrm{i}\kappa_0(R+R_s)}ds_1ds_2 \tag{13}$$

The integrand function is now independent of the large parameter κ_0, except in the phase function. The integration variables, s_1 and s_2, as shown in Fig. 1, appear in the surface coordinate $\mathbf{y}=\mathbf{y}(s_1, s_2)$.

III. Asymptotic Analysis

The asymptotic analysis to extract the diffracted pressure from the result (13) starts with conceptually applying the method of stationary phase to the double integral. The method is applicable because the integrand function contains a gradually varying amplitude function and a rapidly varying phase function for large values of κ_0. In this limit, the rapid oscillations of the exponential factor result in mutual cancellations of the contributions from the individual surface integration elements, except at the location of **y** where the gradients of the phase function vanish, at which the cancellations are not complete. This is the essence of the method of stationary phase, which is a well-known mathematical method [18, 25] so that no details are given here. The application of this method to the surface integral in (13) leads to contributions from the stationary points, which are the physical reflection points on the surface, and a contour integration along the boundaries of the surface area. The former is the reflected pressure discussed in [17], discarded here since the focus of the derivation is the diffracted field. The latter is the diffracted pressure if the scattering body contains sharp edges, which are geometrical discontinuities, and thus, constitute portions of the integration contour.

The contour integration is the result of the method of integration by parts for double integrals, namely, the divergence theorem. To proceed, it is convenient to denote the amplitude of the integrand function by

$$f(\mathbf{y})=\frac{1}{R_s R}\left[\mathbf{n}\cdot\nabla R+\frac{\rho_0 c_0}{\beta^2 Z}\left|\nabla R_s-\mathbf{M}\right|^2\right]\left(1+C_R+C_D\right) \tag{14}$$

and the phase function by

$$\psi(\mathbf{y})=R+R_s \tag{15}$$

both being a function of the curvilinear coordinates s_1 and s_2 through the surface coordinate $\mathbf{y}=\mathbf{y}(s_1, s_2)$. With these, the result (13) can be rewritten as

$$p_D(\mathbf{x}) = \frac{\mathrm{i}\kappa_0 q_0 e^{-\mathrm{i}\kappa_0(\mathbf{x}-\mathbf{x}_s)}}{(4\pi)^2} \int_{S(\mathbf{y})} f(\mathbf{y}) e^{\mathrm{i}\kappa_0\psi}\, ds_1 ds_2 \ . \tag{16}$$

To facilitate the integration, it is straightforward to show that,

$$f(\mathbf{y})e^{\mathrm{i}\kappa_0\psi} = \frac{1}{\mathrm{i}\kappa_0}\tilde{\nabla}\cdot\left(f(\mathbf{y})e^{\mathrm{i}\kappa_0\psi}\frac{\tilde{\nabla}\psi}{\left|\tilde{\nabla}\psi\right|^2}\right) + O\left(\frac{1}{\kappa_0^2}\right) \tag{17}$$

by simple differentiation, where the gradient operator is with respect to the curvilinear coordinates,

$$\tilde{\nabla} = \left\{ \frac{\partial}{\partial s_1}, \frac{\partial}{\partial s_2} \right\} \tag{18}$$

is the gradient operator with respect to the curvilinear coordinates s_1 and s_2. Thus, the integrand function in the result (16) is in the form of a divergence to the leading order in the parameter $1/\kappa_0$. The application of the divergence theorem then leads to

$$p_D(\mathbf{x}) = \frac{q_0 e^{-\mathrm{i}\kappa_0(\mathbf{x}-\mathbf{x}_s)}}{(4\pi)^2} \int_{C(\mathbf{y})} f(\mathbf{y}) \frac{\tilde{\nabla}\psi\cdot\mathbf{n}_c}{\left|\tilde{\nabla}\psi\right|^2} e^{\mathrm{i}\kappa_0\psi}\, ds \tag{19}$$

where $C(\mathbf{y})$ collectively denotes the sharp edges with $\mathbf{n}_c$ being the principal unit normal of the edges, lying in the surface S and pointing outward, and with differential arc length ds. The application of the divergence theorem to (16) leads to contour integrations of along closed curves, of which only the sharp-edge segments are needed to extract the sharp-edge diffraction.

The result (19) is the diffracted pressure by the sharp edges. It can in principle be calculated by numerical integration. At high frequencies, the integration contour may be hundreds of wavelengths long and the integrand function is highly oscillatory. The accurate integration critically depends on accurate cancellations due to the phase oscillations. This numerical challenge is an advantage for the use of the stationary phase method again, but now applied to the single-contour integration, giving the leading-order solution to the diffracted pressure. In practical applications, the sharp edges may be discontinuous, either in the contour itself, or in its slope, or both. In this case, the collective contour C is given by a set of contour segments, which may be of any shape. In terms of the integration arc length s, each segment starts at $s=s_a$ and ends at $s=s_b$. Thus, the result (19) can be rewritten as

$$p_D(\mathbf{x}) = \frac{q_0 e^{-\mathrm{i}\kappa_0(\mathbf{x}-\mathbf{x}_s)}}{(4\pi)^2} \sum_{n=1}^{N} \int_{s_a}^{s_b} f(\mathbf{y}) \frac{\tilde{\nabla}\psi\cdot\mathbf{n}_c}{\left|\tilde{\nabla}\psi\right|^2} e^{\mathrm{i}\kappa_0\psi(s)}\, ds \tag{20}$$

in which N is the total number of segments and both s_a and s_b are a function of the segment number n.

The leading-order solution from each segment integration consists of the contribution from the stationary phase point on the segment and the two end points of the segment. The stationary phase point is determined by the vanishing of the derivative of the phase function, namely, by

$$\psi'(s) = 0 \tag{21}$$

where the prime indicates differentiation with respect to the contour arc length s. This equation is to be solved for the arc length s with the solution denoted by $s=s^*$. The stationary phase point is of course different for different edge segments, and hence, to be understood as a function of the segment number n, which is also the case for the end points $s=s_a$ and $s=s_b$. In general, the leading-order solution is given by three contributions, one from the stationary phase point and two from the segment ends. The method is standard with the result,

$$p_D(\mathbf{x}) = \frac{q_0 e^{-\mathrm{i}\kappa_0(\mathbf{x}-\mathbf{x}_s)}}{(4\pi)^2} \sum_{n=1}^{N}\sum_{k=1}^{3} A(s_k) f(s_k) \frac{\tilde{\nabla}\psi\cdot\mathbf{n}_c}{\left|\tilde{\nabla}\psi\right|^2} e^{\mathrm{i}\kappa_0\psi(s_k)} \tag{22}$$

where the inner summation of k=1 to 3 accounts for the three contributions from the segment integration and the outer summation of n = 1 to N collects contributions from all edge segments. The three contributions are evaluated at

$$s_k = \left\{ s^*, s_b, s_a \right\} \tag{23}$$

respectively for the three terms of k=1,2,3 and the quantity A is introduced to save writing, with the three corresponding terms defined by

$$A(s_k) = \left\{ \sqrt{\frac{2\pi}{\kappa_0\left|\psi''(s^*)\right|}} e^{\mathrm{i}[\mathrm{sig}(\psi'')\pi/4]},\ \frac{1}{\mathrm{i}\kappa_0\psi'(s_b)},\ -\frac{1}{\mathrm{i}\kappa_0\psi'(s_a)} \right\}. \tag{24}$$

For a curved edge segment, there may be multiple stationary phase points, in which case, the first term in the result for k=1 should be understood as the summation of contributions from all stationary phase points. In the case where a segment does not contain a stationary phase point, the result is then given only by the contributions of the two end points of the edge segment.

The result (22) is a general solution to the diffracted pressure including effects of arbitrary edge shape, mean flow and surface impedance. It is an explicit algebraic formula. To facilitate the calculations of the quantities and to reveal the diffraction features, explicit expressions can be derived for the terms in the solutions. This can start with the derivative of the phase function,

$$\psi'(s) = R' + R_s' = \nabla(R + R_s)\cdot\mathbf{y}'(s)\,. \tag{25}$$

For curvilinear coordinates, the derivative of the surface coordinate $\mathbf{y}$ with respect to the arc length s is simply the unit tangential vector of the contour, denoted by $\mathbf{s}$=$\mathbf{y}'(s)$. With this and the expansion of the gradients, it follows that,

$$\psi'(s) = \beta^2\left(\frac{\mathbf{y}-\mathbf{x}}{R}+\frac{\mathbf{y}-\mathbf{x}_s}{R_s}\right)\cdot\mathbf{s} + \mathbf{M}\cdot\mathbf{s}\left(\frac{\mathbf{y}-\mathbf{x}}{R}+\frac{\mathbf{y}-\mathbf{x}_s}{R_s}\right)\cdot\mathbf{M} \tag{26}$$

This can be used to calculate the last two terms in (25) since all quantities are explicit with $\mathbf{y}$ substituted by its values at the two end points of the edge segments. It can also be used to find the stationary phase point by setting it to zero, which leads to an equation that depends on the specific form of the diffraction contour represented by $\mathbf{y}(s)$. The vanishing of (25) defines the mathematical points of stationary phase, which are precisely the physical points of diffraction on the edge. This becomes clear once it is recognized that R and R_s are the radii of curvatures of the diffracted and the incident wave front, respectively. Thus, the vanishing (25) simply states that the angle between the propagation direction of the incident sound and the edge tangential at the diffraction point must be equal to the angle between the propagation direction of the diffracted waves and the edge tangential. This is precisely the Fermat's principle of wave propagation along the shortest path.

The leading-order term in (24), and hence, the diffracted pressure (22), is the first term, corresponding to the diffraction at the diffraction point on the edge. It is inversely proportional to the square root of the acoustic wavenumber, or frequency, which makes it a smaller contribution in comparison with the incident and the reflected pressures that are both of order one. Thus, the contribution represented by the diffraction coefficient C_D in (14) can be omitted in consistency with the high-frequency asymptotic analysis.

The calculation of the diffracted pressure from the stationary phase point, given by the term of k=1 in (22), also requires the second derivative of the phase function ψ evaluated at the stationary phase point. It can be found by further differentiating the result (25) with respect to s, leading to

$$\psi''(s) = \nabla(R + R_s)\cdot\mathbf{y}''(s) + \left(\frac{1}{R}+\frac{1}{R_s}\right)\left[\beta^2 + (\mathbf{M}\cdot\mathbf{s})^2\right] - \frac{(\nabla R\cdot\mathbf{s})^2}{R} - \frac{(\nabla R_s\cdot\mathbf{s})^2}{R_s}\,. \tag{27}$$

This general result can be simplified when evaluated at the stationary phase point by making use of the result (26), set to zero, which results in

$$\psi''(s) = \nabla(R + R_s)\cdot\mathbf{y}''(s) + \left(\frac{1}{R}+\frac{1}{R_s}\right)\left[\beta^2 + (\mathbf{M}\cdot\mathbf{s})^2 - (\nabla R\cdot\mathbf{s})^2\right]. \tag{28}$$

The gradient operations with respect to the curvilinear coordinates s_1 and s_2 in the result (22) can be related to the gradients with respect to $\mathbf{y}$, which are denoted by ∇, because s_1 and s_2 appear in the quantities in the integrand only through $\mathbf{y}$. By the rule of chain differentiation,

$$\tilde{\nabla}\psi = \left\{\nabla\psi\cdot\frac{\partial\mathbf{y}}{\partial s_1}, \nabla\psi\cdot\frac{\partial\mathbf{y}}{\partial s_2}\right\} = \left\{\nabla\psi\cdot\mathbf{s}_1, \nabla\psi\cdot\mathbf{s}_2\right\} \tag{29}$$

where the last step follows from the definition that the derivatives of the surface coordinates $\mathbf{y}$ with respect the curvilinear coordinates s_1 and s_2 are simply the unit tangent vectors of the curvilinear arcs, denoted by $\mathbf{s}_1$ and $\mathbf{s}_2$, respectively. The surface curvilinear coordinates $\mathbf{s}_1$ and $\mathbf{s}_2$ in the local region near the edge contour can be conveniently chosen to be the contour tangent $\mathbf{s}$ and its outward normal $\mathbf{n}_c$. It follows that

$$\tilde{\nabla}\psi\cdot\mathbf{n}_c = \nabla\psi\cdot\mathbf{n}_c \tag{30}$$

and the squared amplitude of the phase function gradient in the curvilinear coordinate system becomes,

$$\left|\tilde{\nabla}\psi\right|^2 = \left(\nabla\psi\cdot\mathbf{s}\right)^2 + \left(\nabla\psi\cdot\mathbf{n}_c\right)^2. \tag{31}$$

Here all gradient operations are with respect to the surface coordinate **y**, which is a function of the contour arc length *s*. For calculating the contributions from the end points of the segments, the two results above can be directly substituted into (22) so that

$$\frac{\tilde{\nabla}\psi\cdot\mathbf{n}_c}{\left|\tilde{\nabla}\psi\right|^2}=\frac{\nabla\psi\cdot\mathbf{n}_c}{\left(\nabla\psi\cdot\mathbf{s}\right)^2+\left(\nabla\psi\cdot\mathbf{n}_c\right)^2} \tag{32}$$

and for the contributions from the stationary phase points, the result can be simplified further because the first term on the right-hand side of (31) is identically zero from the definition of the stationary phase point so that

$$\frac{\tilde{\nabla}\psi\cdot\mathbf{n}_c}{\left|\tilde{\nabla}\psi\right|^2}=\frac{1}{\nabla\psi\cdot\mathbf{n}_c}\,. \tag{33}$$

The substitution of the above results into (22) then leads to the solution for the diffracted pressure as an explicit analytical formula,

$$p_D(\mathbf{x})=\frac{q_0 e^{-\mathrm{i}\kappa_0(\mathbf{x}-\mathbf{x}_s)}}{(4\pi)^2}\sum_{n=1}^{N}\sum_{k=1}^{3}A(s_k)f(s_k)\frac{1}{\nabla\psi\cdot\mathbf{n}_c}e^{\mathrm{i}\kappa_0\psi(s_k)}\,. \tag{34}$$

IV. Singularity Treatment

The integral representation of the Green's theorem formulation for the diffracted pressure given by (16) is well-behaved and regular, a manifestation of the well-posed physical problem of sound scattering. However, there are two types of potential singularities in the first-order asymptotic solutions (34), both due to the application of the mathematical method of stationary phase to the leading order in the asymptotical analysis. Thus, the singularities are not inherent of the physical problem and are only present for the first-order asymptotic solutions. The singularities can be treated, either by expanding the analysis to a higher order to eliminate the singularities, or by replacing a mathematically singular function with a regular function. In both cases, the treatment regulates the behavior of the solution in the small range of the parametric space near the singularities while keeping the solution unchanged elsewhere. The details of the singularity treatments will be illustrated in this section for both approaches.

The asymptotic solution (34) has singularities when the denominator vanishes. The singularities result entirely from the derivations of the surface integration discussed in the previous section where the divergence theorem is used to find the diffracted field. The singularities can be treated to render the solution valid in the entire parametric space once the nature of the singularities is identified. To this end, the phase function (15) can be used to calculate the denominator term, which is denoted by Δ and can be cast in the form of the product of two vectors,

$$\Delta=\nabla\psi\cdot\mathbf{n}_c=\left(\frac{\mathbf{y}-\mathbf{x}}{R}+\frac{\mathbf{y}-\mathbf{x}_s}{R_s}\right)\cdot\left[\beta^2\mathbf{n}_c+\left(\mathbf{M}\cdot\mathbf{n}_c\right)\mathbf{M}\right]. \tag{35}$$

Thus, the denominator vanishes if one of the two conditions is satisfied, namely, the first vector is zero or the product of the two vectors is zero. The second vector is essentially the principal normal of the edge, slightly modified by the mean flow, which is nonzero itself. The first condition is simply the grazing coincidence condition where the incident wave direction exactly aligns with the diffracted waves. This is the direction that separates the insonified region and shadow region. The second condition also has a physical meaning. Since the principal normal of the edge is perpendicular to the surface normal, by definition, the product of the two vectors is zero only if the first vector is parallel to the surface normal, which, by the Snell's law of reflection, implies that the direction of diffracted wave is parallel to the direction of the reflected wave by the surface at the edge. Thus, the second condition for singularities is the boundary of the reflected wave. The singular behavior at these conditions is well known in geometric acoustics and represents discontinuities in the leading-order solutions of individual wave components at the boundaries of various wave regions. However, the physical quantity of the total wave field is always continuous, and the diffraction is known to behave like the Fresnel function in the transition region.

Thus, the Fresnel function can be used to regulate the solutions for the diffracted pressure. Symbolically, the singular term and the phase term in the result (34) can be written as

$$\frac{1}{\Delta}e^{\mathrm{i}k_0\psi}=\frac{1}{\Delta}e^{\mathrm{i}k_0\psi_0}e^{\mathrm{i}k_0(\psi-\psi_0)}\,. \tag{36}$$

The phase function at the singularity is denoted by ψ_0, namely,

$$\psi_0=\psi\big|_{\Delta\to 0}=(1+a\Delta^2)\psi \tag{37}$$

where a is a constant whose value only affects the rate of transition in the small range near the singularity but does not have any impact on the overall solution. A transformation can be defined by

$$\eta^2 = \frac{2}{\pi} k_0 \left(\psi_0 - \psi \right) \tag{38}$$

so that the phase function term in (37) can be transformed to

$$e^{\mathrm{i}k_0(\psi-\psi_0)} = e^{-\mathrm{i}\pi\eta^2/2} . \tag{39}$$

By the definition of the Fresnel function, its asymptotic form at large argument is given by

$$F(\eta) = \mathrm{sgn}(\eta)\frac{1+\mathrm{i}}{2} + \frac{1}{\mathrm{i}\pi\eta} e^{\mathrm{i}\pi\eta^2/2} \tag{40}$$

where sgn is the sign function. This can be combined with (38) with the result substituted into (36), yielding

$$\frac{1}{\Delta} e^{\mathrm{i}k_0\psi} = -\frac{\mathrm{i}\pi\eta}{\Delta} e^{\mathrm{i}k_0\psi_0} \left[F^*(\eta) - \mathrm{sgn}(\eta)\frac{1-\mathrm{i}}{2} \right]. \tag{41}$$

with the asterisk on the Fresnel function indicating the complex conjugate. The transformation quantity η can be found by substituting (37) into (38), leading to

$$\eta = \Delta\sqrt{\frac{2k_0\psi a}{\pi}} . \tag{42}$$

The singular term denoted by (36) then becomes,

$$\frac{1}{\Delta} e^{\mathrm{i}k_0\psi} = -\mathrm{i}e^{\mathrm{i}k_0\psi_0}\sqrt{2\pi k_0\psi a}\left[F^*(\eta) - \mathrm{sgn}(\eta)\frac{1-\mathrm{i}}{2} \right]. \tag{43}$$

The right-hand side of this result, and hence, the diffracted pressure (34), is free from the singularity due to the vanishing of the quantity Δ, regulated by the Fresnel function.

The use of a regular function that represent the physical behavior of the wave field to eliminate the singularities is one of the two methods to regulate the first-order solutions of the asymptotic analysis. Since the singularities are entirely due to the use of the asymptotic analysis, the method itself can also be used to ensure regular solutions, by carrying out the analysis to the next order to capture the leading-order contributions. This is illustrated here by the singularity in the first term in the result (24), which occurs when the second derivative of the phase function vanishes. This singularity can be traced back to the Taylor series expansion of the phase function in the application of the stationary phase method, in which the second derivative is considered as the leading-order term. However, when it is nearly zero, it should not be considered as leading order. Instead, the expansion should be carried out to the next true leading-order term. The expansion is in the form of

$$\int_{-\infty}^{+\infty} e^{\mathrm{i}k_0\psi(s)} ds = e^{\mathrm{i}k_0\psi(s^*)} \int_{-\infty}^{+\infty} e^{\mathrm{i}k_0\left[\psi'(s^*)(s-s^*)+\frac{1}{2}\psi''(s^*)(s-s^*)^2+\frac{1}{6}\psi'''(s^*)(s-s^*)^3+\cdots\cdots\right]} ds \tag{44}$$

where the phase function $\psi(s)$ is expanded at the stationary phase point $s=s^*$ and the number of primes on the phased function indicates the order of the derivative with respect to s. The first derivative is zero by the definition of the stationary phase method. If the second derivative is also zero or very small, the leading-order term is the third derivative. Thus, the asymptotic analysis should include this term and the result can be derived as

$$\int_{-\infty}^{+\infty} e^{\mathrm{i}k_0\psi(s)} ds = e^{\mathrm{i}k_0\psi(s^*)} \int_{-\infty}^{+\infty} e^{\mathrm{i}k_0\frac{1}{6}\psi'''(s^*)(s-s^*)^3} ds = \frac{\Gamma(1/3)}{\sqrt{3}} e^{\mathrm{i}k_0\psi(s^*)} \left(\frac{6}{k_0\left|\psi'''(s^*)\right|} \right)^{\frac{1}{3}} \tag{45}$$

where Γ is the Gamma function. This result is apparently free of the singularity due to the vanishing of the second derivative. Theoretically, there is still the possibility that the asymptotic result to this order becomes singular, if the third derivative of the phase function also vanishes. This is, however, not likely in practical applications, because it requires three orders of derivatives of the phase function to vanish at the same location. Furthermore, the expansion in (45) can be carried out to any order until a nonzero term is found. Thus, the method provides a way to avoid singularities in the diffraction solution.

V. Validation

The NACA 0012 airfoil has been used in an extensive experimental study for sound scattering [26] in the NASA Quiet Flow Facility (QFF), providing a database for validating prediction tools and methods [16-18]. The configuration used in the experimental study is described in [26], which involves an airfoil with a straight trailing edge

and rigid airfoil surface. The source for the scattering is produced by a laser spark, forming an impulsive minimally intrusive point source. The sound waves generated by the source are highly coherent. Though the test data only represent a special simplified configuration, the data can still serve as a first step of validation for the method derived here. Furthermore, the simple geometry will be used in the subsequent sections as a baseline for comparisons where variations will be introduced for the trailing edge shape, the mean flow, and the surface impedance. The configuration for the validation is illustrated in Fig. 2. The airfoil has a chord length of 0.2 m. The source, indicated by the blue circle, is on the top side of the airfoil, located at 75% of the airfoil chord from its leading edge and at 0.025 m from the airfoil surface. The open circles are source locations used in the test but are not used here. The measurement locations are below the airfoil on the opposite side of the source, indicated by the gray and black dots. They are one airfoil chord below the airfoil centerline. The black dots are locations for which spectral comparisons will be shown and the gray dots indicate locations for spatial trend comparison. The validation examples are for zero angle of attack and for a mean flow Mach number of 0.16.

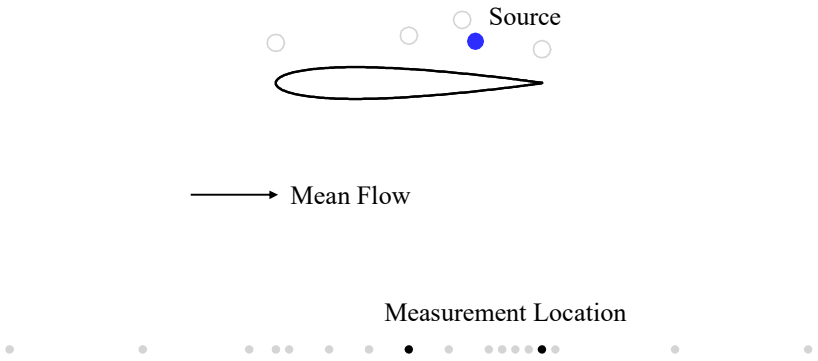

Fig. 2 Illustration of test configuration in QFF for validation.

The spectral comparisons between predictions and data are shown in Fig. 3, respectively at the mid-chord location (left plot), and the trailing edge location (right plot). The measurement locations for the two plots are indicated by the black dots in Fig. 2. The plots are for the spectrum of the scattering pressure, normalized by the incident pressure spectrum and denoted by ΔSPL as a function of frequency. The red solid curves are the predictions, and the green dashed curves are the experimental data. Both the amplitudes of the scattered pressure and the interference patterns, resulting from the diffractions from the leading and the trailing edges of the airfoil, are well captured by the predictions, with the spectral peaks and dips well aligned between the data and the predictions. There are spectral humps in the experimental data at high frequencies above 30 kHz. These are artifacts due to the nose cone response of the microphone, and thus, should be discarded in the comparisons.

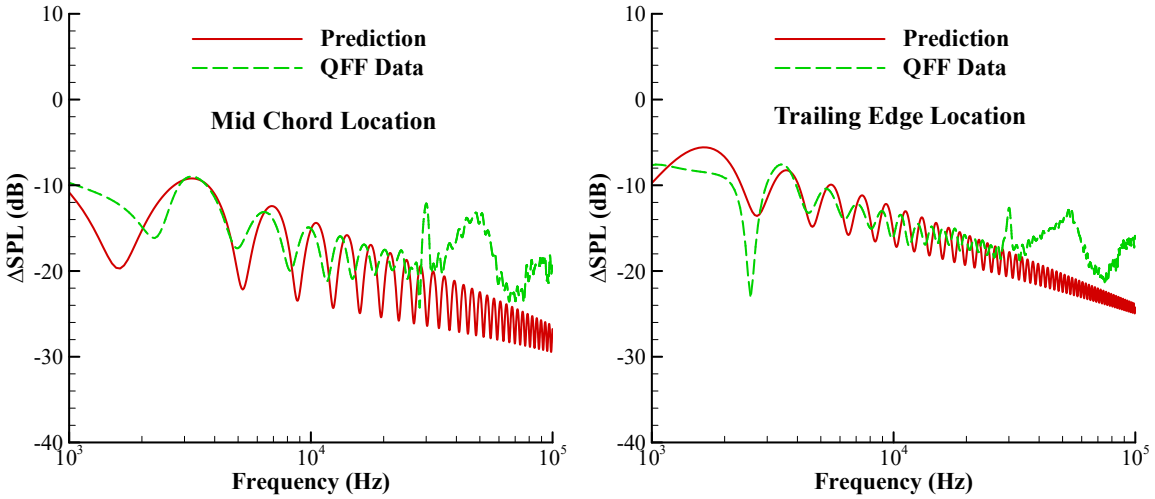

Fig. 3 Spectral comparison at the mid-chord (left) and trailing edge (right) location.

Because of the highly coherent laser spark source, there are strong interferences between the two diffraction components, as manifested by the spectral peaks and dips in frequency. The interferences are also present in the spatial

domain. This is illustrated in Fig. 4, where the plotted quantity is the octave band spectrum, normalized by the incident sound spectrum, and again, denoted as ΔSPL, with the left diagram for the 7 kHz band and the right for the 14 kHz band. The horizontal axis is the flow-direction coordinate, normalized by the airfoil chord length so that the leading edge is at zero and the trailing edge is at one. The comparisons in Fig. 4 show that the measurements do not have enough spatial resolution to capture the sharp variations due to the interferences, which are well captured by the predictions. At the locations of the measurements, the two agree very well. The validation cases only cover one of the three features emphasized in developing the method presented here, namely, only the effect of mean flow. The other two are the noncanonical edge shape and surface impedance. Thus, the validation can only be considered as the first step. More complete tests with edge-shape variations and surface treatment are currently planned and will be reported in the future.

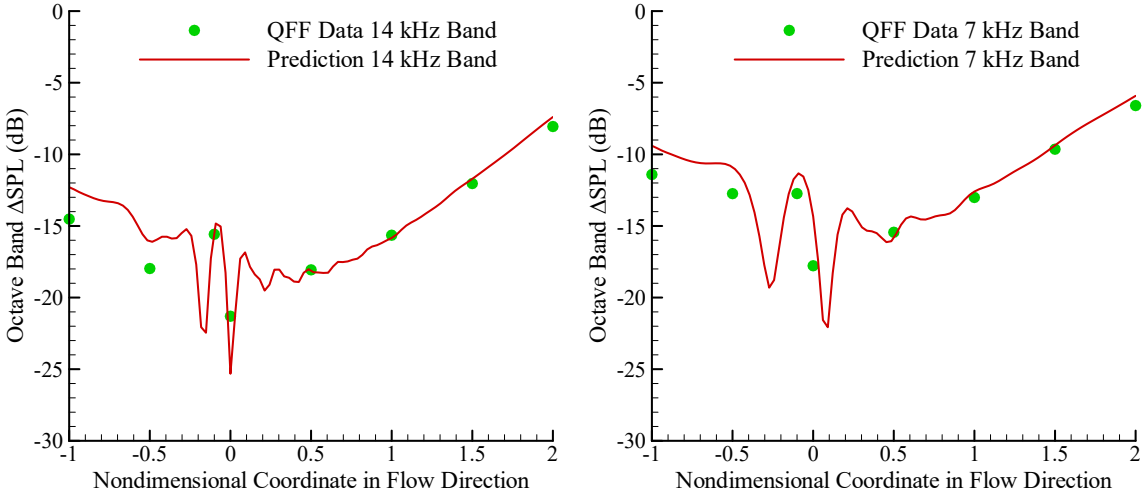

Fig. 4 Spatial scattering pattern for the 7 kHz (left) and the 14 kHz (right) octave band.

VI. Illustration of Parametric Variations

The simple geometry of the NACA 0012 airfoil will be used to illustrate the effects of the parametric variations of the sharp trailing edge. The baseline is defined to be the airfoil with a straight trailing edge and the variations in the edge shape include a section of the trailing edge replaced by a wavy shape. To follow the experimental setup discussed in the previous section, the geometry of the parametric variations is illustrated in Fig. 5. The baseline airfoil, the microphone locations below the airfoil, and the source position are the same as those in the previous section. In addition to the variations in the trailing edge shape, a line of microphone locations is added above the airfoil on the same side as the source, often referred to as the insonified region. This is used to illustrate later in this section the effect of the edge diffraction when other sound scattering components are present.

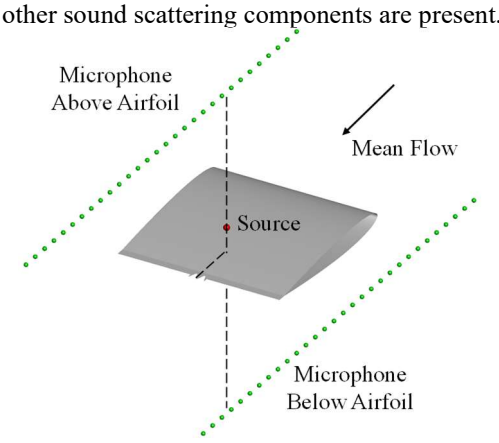

Fig. 5 Geometry for edge feature parametric studies.

The modification of the trailing edge from a straight edge to noncanonical shapes is by a set of wavy shapes. Some examples are shown in Fig. 6, together with the baseline. The three wavy shapes are respectively named the recessed, the mean, and the protruding shape, according to their relative position to the nominal straight edge. The recessed

shape has the tip of the wavy pattern aligned with the nominal straight edge so that the entire wave pattern is upstream of the straight edge. The mean wavy shape is designed by shifting the recessed shape in the downstream direction by half of the wavy height, making the mean position of the wavy pattern at the straight edge position. The mean wavy edge and the straight edge have the same wetted area. The protruding shape is designed by shifting the mean wavy shape further downstream by another half of the height so that the entire wavy pattern is downstream of the straight edge. In all three cases, the height of the wavy patterns is 0.01 meters, equal to 5% of the baseline airfoil chord. The aspect ratio, defined by the pattern wavelength divided by its height, is one for the three configurations in the figure.

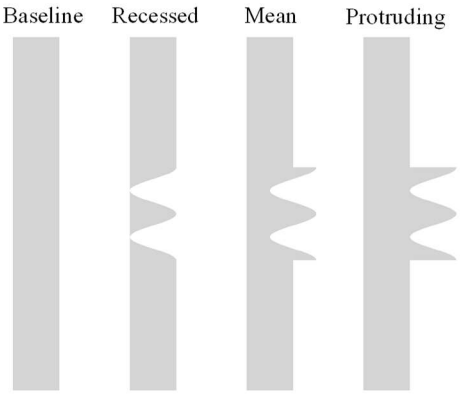

Fig. 6 Illustration of trailing edge baseline and wavy shapes.

Comparisons among various edge shapes are given in Fig. 7, which shows the diffracted sound from an incoherent source in the left diagram and a coherent source in the right diagram, both normalized by the incident sound and plotted as a function of the microphone location along the line below the airfoil on the opposite side to the source, as shown in Fig. 5. The flow direction coordinate is normalized by the airfoil chord so that the leading edge is at zero and the trailing edge is at one. The range of the results extends two chords upstream of the airfoil leading edge and two chords downstream of its trailing edge. Since the sound pressure is normalized by the incident sound, removing the effect of propagation distance, the plots can also be regarded as directivity of the diffracted sound, with a range in polar angle from about 22 degrees to about 158 degrees, measured from the upstream direction. The results shown in the figure are for a rigid-edge surface with the mean flow Mach number of 0.2 at 10 kHz frequency, the frequency being high to account for the small dimensions of the airfoil.

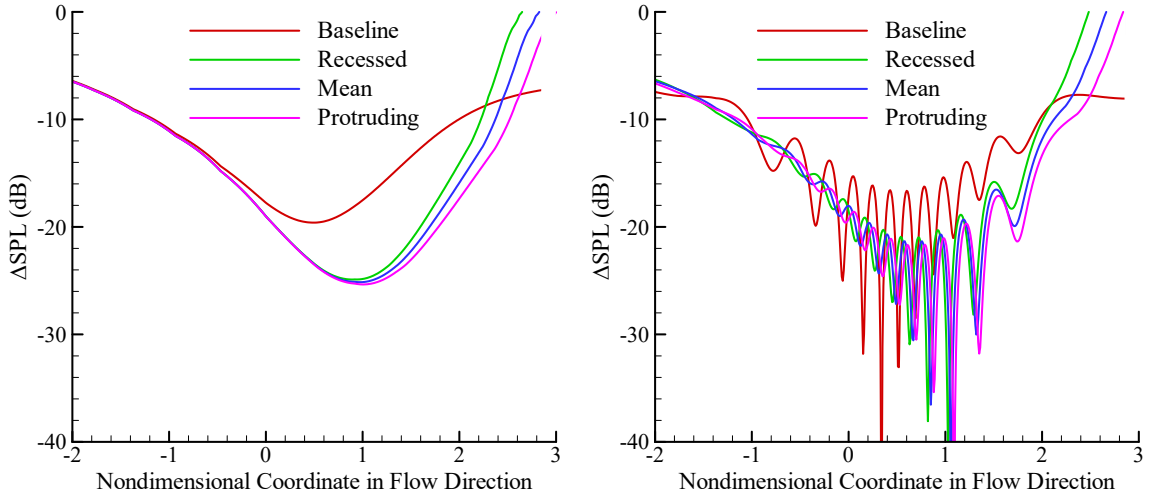

Fig. 7 Comparisons for edge-shape effect for incoherent (left) and coherent (right) source.

An interesting feature of the results shown in Fig. 7 is the noise reduction by the wavy trailing edge, in comparison to the straight edge, by up to 7 dB in the approximate range from the airfoil leading edge position to one airfoil chord downstream of it trailing edge, corresponding to an approximate polar angle range from 65 to 145 degrees. The noise reduction is achieved by all three wavy shapes with small variations among them in this spatial range, even for the recessed shape that has the same shadow region as the straight-line edge, for the microphone line used here. The increased shadow region for the mean and the protruding edge is responsible for the small variations among the wavy

shapes in this spatial range. Further downstream outside this range, the variations among the wavy shapes become more noticeable and all of them become noisier than the baseline at very downstream locations. These features can be explained by the number of diffraction points on the edge, their relative locations, and the relative positions between the source and the microphone. For example, the mean wavy edge has a diffraction point that is at the same location as a straight edge, but because the curvature at this point on the wavy edge is larger than that on the straight edge, the diffraction by the wavy edge is less efficient than the straight edge, even if the two have a diffraction point at the same physical location. For the wavy edges, there are also two additional diffraction points near the two troughs of the wavy pattern. The added diffractions from these additional diffraction points are mostly overwhelmed by the reductions due to the curvature change, unless the microphones are in the far downstream locations where the three diffraction points coalesce, and the curvature effect becomes small.

The impact of the edge shape on total sound scattering depends on the presence of other scattering components and their relative ranking order of importance. In general, the total sound includes the direct radiation from the source and the reflection from the scattering body, as well as the diffractions. In the shadow region below the airfoil, the scattered field is given by the diffractions from both the leading and the trailing edge, respectively at the coordinate 0 and 1 for the results shown in Fig. 7. The trailing edge shape mostly affects the downstream locations. In Fig. 7, the results for the group of wavy edges only slightly differ from each other near and upstream of the leading edge, because the dominant diffraction in this region is the smooth-surface diffraction at the airfoil leading edge, independent of the trailing edge shape. The edge shapes can change the phase of the diffraction from the trailing edge so that, for the coherent source, more noticeable variations in the results are seen in the right diagram of the figure, even in the upstream locations, due to interferences between the two diffractions.

The effect of edge shape in the presence of other scattering components is further illustrated in Fig. 8 by the total sound at microphone locations above the airfoil, normalized by the incident sound and plotted for all the wavy edges, as well as the baseline. The effect of the edge shapes is small because the direct radiation and the reflection are the dominant components at these microphone locations.

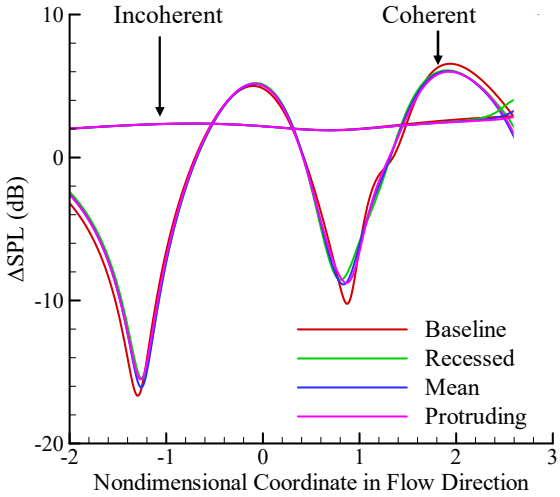

Fig. 8 Comparisons for edge-shape effect in insonified region above airfoil.

In Fig. 8 and between the two plots in Fig. 7, the differences between coherent and incoherent sources are clearly shown. The coherence is an important feature in aircraft noise source characteristics, and is a feature that needs to be captured by propagation and scattering methods because it can significantly affect the sound amplitude and its directivity, namely, its spatial distribution pattern, as clearly illustrated in Fig. 8 and Fig. 7. Since both figures are for a discrete frequency of 10 kHz, it is worth pointing out that integration in a finite frequency band should not and cannot be used to eliminate the interference patterns in the coherent source results, in hope of eliminating the differences between the two kinds of sources. The coherent source would correspond to tonal noise in aircraft engine noise applications where the tones are at discrete frequencies and frequency band integration is not appropriate. Even in the highly idealized and artificial case of coherent sound in a frequency band, such as the laser spark source used in the experimental study discussed in the previous section, the frequency band integration smooths out some rapid variations but cannot eliminate the interferences, as is clearly shown in Fig. 4 by both the experimental data and the predictions.

The effect of mean flow on edge diffraction is illustrated in Fig. 9, for the baseline edge in the left diagram and the mean wavy edge in the right diagram, both for an incoherent source, characterized by the smooth spatial variations.

The results are for the microphones in the shadow region below the airfoil for various values of the mean flow Mach number and the source is again at 10 kHz frequency. The variations in the sound levels show a range up to 4 dB in the upstream direction and about 2 dB in the downstream direction, both being noise increase with flow Mach number.

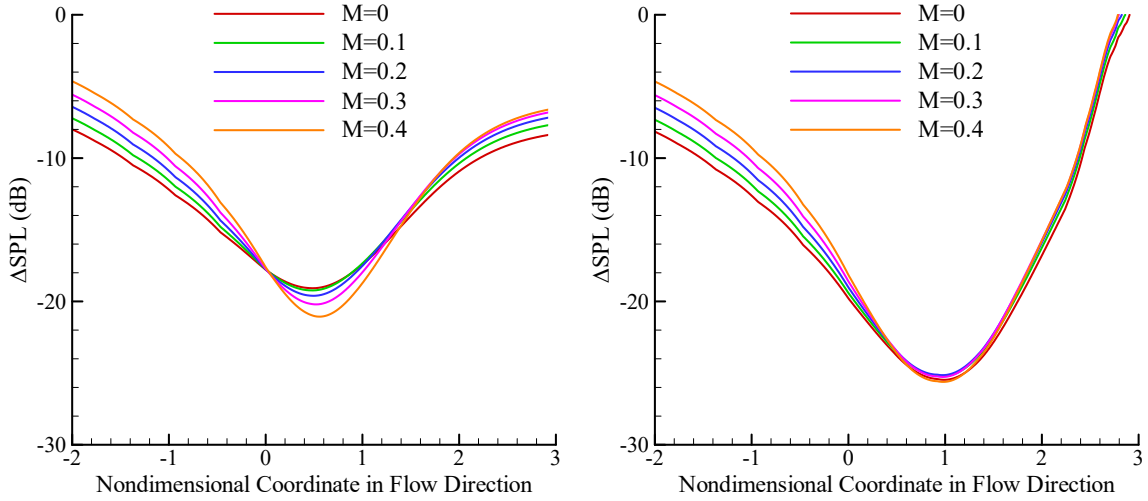

Fig. 9 Effect of mean flow on baseline (left) and mean wavy (right) edge for incoherent source.

The propagation from incoherent sources has no phase information, and hence, no interferences between various components. For coherent sources, however, the changes in noise levels at fixed microphone locations can be significantly affected by the interferences. This is illustrated in Fig. 10, which has the same format and diffraction configuration as in Fig. 9, except that the source is now coherent, which is evident by the peaks and dips in the results. The mean flow changes the propagation phase so that the interference patterns noticeably shift. This amplifies the effect of the mean flow on the sound levels at fixed spatial locations. In the region near and downstream of the trailing edge, the variations in sound levels can reach 6 to 10 dB, due to combined effect of amplitude changes by the mean flow and the shift in the peaks and dips in the interference patterns from one Mach number to another.

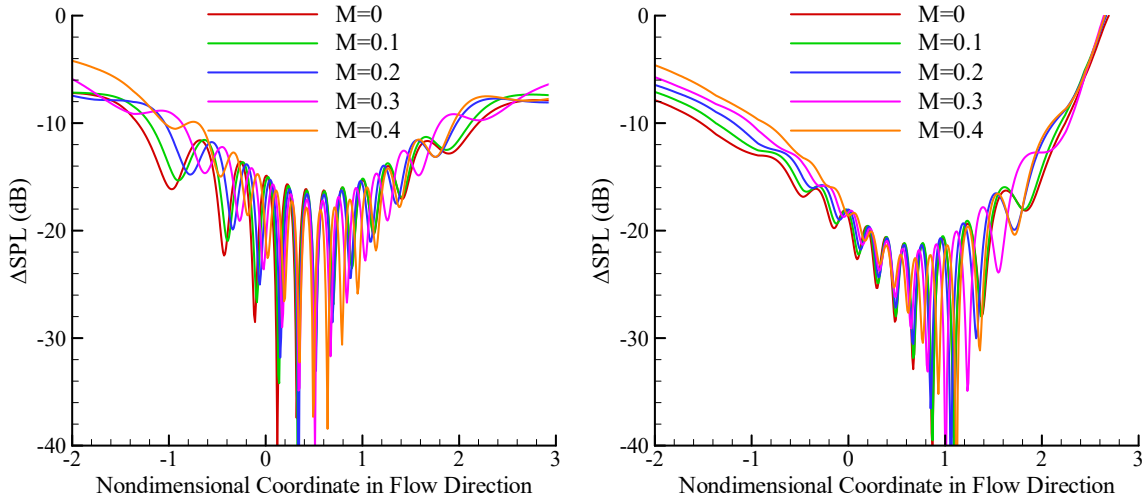

Fig. 10 Effect of mean flow on baseline (left) and mean wavy (right) edge for coherent source.

Most of the sharp edges in aircraft noise applications can be considered as being rigid, such as the wing trailing edges that are required to be aerodynamically smooth. The concept of noise reduction by treated or impedance surfaces is likely to be relevant only in local regions of the aircraft surfaces in specific conditions. The results derived in this paper provide the capability of predicting the sharp-edge diffraction for treated surfaces. Examples are given in Fig. 11, showing the effects for both the baseline straight edge and the mean wavy edge. The left diagram is for an incoherent source and the right diagram for a coherent source. The surface treatment is modeled by a nondimensional impedance value of (2, -0.5), which is meant to illustrate the impedance effect and not meant to represent any practical liner design. The source location, frequency, and the microphone locations in the shadow region are the same as in

previous figures. The results for the untreated rigid edges are plotted by solid curves, with red for the baseline edge and blue for the mean wavy edge, and the results for the treated edges by the dashed curves with the same color scheme. The noise reduction can be as high as 10 dB at locations downstream of the airfoil in the shadow zone where the sharp-edge diffraction is the dominant feature, and hence, most significantly affected by the edge treatment.

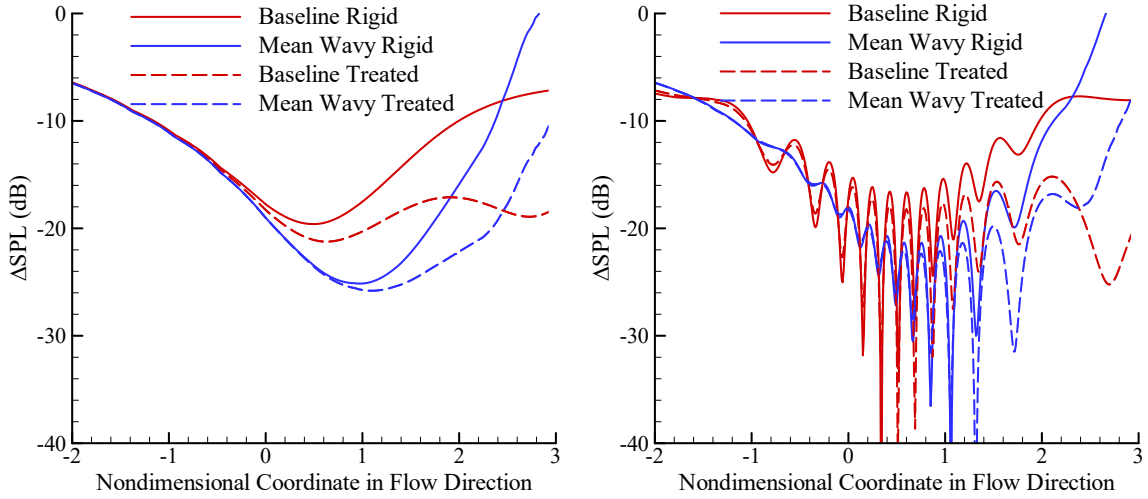

Fig. 11 Impedance effect for incoherent (left) and coherent (right) source.

VII. Summary

A general solution has been derived in this paper for sharp-edge diffraction by noncanonical edge shapes in the presence of mean flow and potential surface impedance on the edge. These are important features for aircraft noise scattering but have not been accounted for in previous studies on sharp-edge diffraction. The solution has been derived, as an explicit analytical formula, by asymptotic analysis in the high-frequency limit, rendering the result applicable to cases in which the acoustic wavelength is smaller than the typical dimension of the scattering body and the edge variations. This is the case for all practical applications of aircraft noise scattering. It is, however, not a strict limitation because the asymptotic method can be used to systematically derive higher-order results, if needed, expanding the validity range of the solutions. It has been shown that the higher-order results can also be used to eliminate singularities in the first-order solution.

The solution has been validated by experimental data for the simple geometry of a NACA 0012 airfoil with a straight trailing edge, as a first step of validation, due to the current availability of data, while more comprehensive and more relevant experimental studies and validation of the method for curved edges and edges with acoustic treatments are planned for future studies.

The airfoil geometry, simple but containing the essential scattering mechanisms such as reflection, smooth-surface diffraction and sharp-edge diffraction, has been used for parametric studies on trailing edge shape, flow Mach number and surface treatment, to illustrate the effects of these edge features and the potential for diffraction control. Results have also been shown for diffractions by both incoherent and coherent sources, which is an important feature in aircraft noise applications, with significant differences in the sound fields between the two. The parametric studies with the simple geometry clearly do not represent any realistic design and applications. Instead, the results are meant to illustrate the edge effects and to demonstrate the capabilities of the new edge diffraction formula in capturing these effects.

Acknowledgments

The support of the NASA Advanced Air Transport Technology Project is gratefully acknowledged.

References

[1] MacDonald, H. M., "A Class of Diffraction Problems," *Proc. Lond. Math. Soc.*, Vol. 14, pp 410-427, 1915.
[2] Bromwich, A., "Diffraction of Waves by a Wedge," *Proc. Lond. Math. Soc.*, Vol. 14, pp 450-463, 1915.
[3] Whipple, F. J. W., "Diffraction by a Wedge and Kindred Problems," *Proc. Lond. Math. Soc.*, Vol. 16, pp 94-111, 1917.
[4] Sommerfeld, A., "Mathematical Theory of Diffraction," *Math. Ann.*, Vol. 47, pp 317-374, 1896.
[5] Ganci, S., "A General Scalar Solution for the Half-plane Problem," *J. Mod. Opt.*, 42(8):1707–1711, August 1995.

[6] Umul, Y. Z., "Young-Kirchhoff–Rubinowicz Theory of Diffraction in the Light of Sommerfeld's Solution," *J. Opt. Soc. Am*. A, 25(11):2734–2742, November 2008.
[7] Morse, P. M., and Ingard, K. U., "*Theoretical Acoustics*," McGraw-Hill, 1968.
[8] Sommerfeld, A., "Lectures on Theoretical Physics," *Optics*, Vol. IV, Academic Press, 1954.
[9] Pierce, A. D., "*Acoustics: An Introduction to its Physical Principles and Application*," McGraw-Hill, 1981.
[10] Keller, J. B., "Geometrical Theory of Diffraction," *J. Opt. Soc. Am*., Vol. 52, No. 2, pp 116–130, 1962.
[11] Lewis, R. M., and Boersma, J., "Uniform Asymptotic Theory of Edge Diffraction," *Math. Phys*., Vol. 10, No. 12, pp 2291–2305, 1969.
[12] Agarwal, A., Dowling, A. P., Shin, H. C., Graham, W., and Sefi, S., "A Ray Tracing Approach to Calculate Acoustic Shielding by the Silent Aircraft Airframe," AIAA Paper 2006-2618, May 2006.
[13] Agarwal, A., and Dowling, A. P., "The Calculation of Acoustic Shielding of Engine Noise by the Silent Aircraft Airframe," AIAA Paper 2005-2996, May 2005.
[14] Lummer, M., "Maggi-Rubinowicz Diffraction Correction for Ray-Tracing Calculations of Engine Noise Shielding," AIAA Paper 2008-3050, May 2008.
[15] Colas, D. F. M., "A Diffraction Integral Based Turbomachinery Noise Shielding Method," Master's Thesis, Department of Aeronautics and Astronautics, Massachusetts Institute of Technology, 2011.
[16] Guo, Y. P., Pope, D. S., Burley, C. L., and Thomas, R. H., "Aircraft System Noise Shielding Prediction with a Kirchhoff Integral Method," AIAA Paper 2017-3196, June 2017.
[17] Guo, Y. and Thomas, R. H., "Geometric Acoustics for Aircraft Noise Scattering," AIAA Paper 2022-3077, June 2022.
[18] Thomas, R.H. and Guo, Y., "Systematic Validation of the PAAShA Shielding Prediction Method," *International Journal of Aeroacoustics*, 2022, Vol. 21(5-7), pp. 558-584.
[19] Guo Y. and Thomas R. H., "System Noise Assessment of Hybrid Wing-Body Aircraft with Open Rotor Propulsion," *J. Aircraft*, **52**(6), 1767-1779, 2015.
[20] Guo Y. and Thomas R. H., "Experimental Study on Open Rotor Noise Shielding by Hybrid-Wing-Body Aircraft," AIAA *Journal*, **54**(1), 242-253, 2016.
[21] June J. C., Thomas R. H., and Guo Y., "System Noise Prediction Uncertainty Quantification for a Hybrid Wing-Body Transport Concept," AIAA *Journal*, **58**(3), 1157-1170, 2020.
[22] Guo Y., Brusniak L., Czech M., and Thomas R. H., "Hybrid Wing Body (HWB) Slat Noise Analysis," AIAA 2013-0462, January 2013.
[23] Bleistein, N., and Handelsman, R. A., "*Asymptotic Expansion of Integrals*," Dover Publications Inc., New York, 1975.
[24] Dowling, A. P., and Ffowcs Williams, J. E., "*Sound and Sources of Sound*," Ellis Horwood Publishers, 1983.
[25] Crighton, D. G., Dowling, A. P., Ffowcs Williams, J. E., Heckl, M., and Leppington, F. G., "*Modern Methods in Analytical Acoustics*," Springer-Verlag, 1992.
[26] Hutcheson, F.V., Bahr, C.J., Thomas, R.H., and Stead, D.J., "Experimental Study of Noise Shielding by a NACA 0012 Airfoil," AIAA Paper 2018-2821, June 2018.